arXiv:1410.0224v1 [physics.chem-ph] 1 Oct 2014

Computer simulation study of surface wave dynamics at the crystal–melt interface.

Jorge Benet, Luis G. MacDowell and Eduardo Sanz
Departamento de Química Física, Facultad de Ciencias Químicas,
Universidad Complutense de Madrid, 28040 Madrid, Spain
(Dated: October 2, 2014)

We study, by means of computer simulations, the crystal-melt interface of three different systems: hard-spheres, Lennard Jones and the TIP4P/2005 water model. In particular, we focus on the dynamics of surface waves. We observe that the processes involved in the relaxation of surface waves are characterized by distinct time scales: a slow one related to the continuous recrystallization and melting, that is governed by capillary forces; and a fast one which we suggest to be due to a combination of processes that quickly cause small perturbations to the shape of the interface (like e. g. Rayleigh waves, subdiffusion, or attachment/detachment of particles to/from the crystal). The relaxation of surface waves becomes dominated by the slow process as the wavelength increases. Moreover, we see that the slow relaxation is not influenced by the details of the microscopic dynamics. In a time scale characteristic for the diffusion of the liquid phase, the relaxation dynamics of the crystal-melt interface of water is around one order of magnitude slower than that of Lennard Jones or hard spheres, which we ascribe to the presence of orientational degrees of freedom in the water molecule. Finally, we estimate the rate of crystal growth from our analysis of the capillary wave dynamics and compare it with previous simulation studies and with experiments for the case of water.

I. INTRODUCTION

The crystal-melt interface (CMI) has a great relevance in materials science given that its properties have a strong influence in crystal nucleation and growth, as well as on wetting phenomena [1, 2]. Despite its importance, the CMI is far less understood than the fluid-fluid interface because the former is difficult to probe with standard experimental techniques like X-ray diffraction [3]. For example, it is well known that the interfacial tension of liquid water at ambient conditions is 72 mN/m, whereas the reported values for the ice-water interfacial free energy at ambient pressure range from to 25 to 35 mN/m [4]. Also the dynamics of the fluid-fluid interface is far better understood than that of the CMI [5, 6]. Understanding the dynamics of the CMI is of great interest given that it can provide valuable insight to the important process of crystal-growth [7, 8].

The CMI interface is not flat, but rather exhibits relatively large undulations of the local interface position, or surface waves (SW), as a result of thermal excitations (see online movie [9]). For length scales below the capillary length, SW are mainly governed by the interfacial stiffness and are known under the name of capillary waves (CW). The equilibrium and dynamic properties of CW at the fluid–fluid interface have a long history and were already studied by Smoluchowski and Kelvin [10, 11]. For the CMI, the study of the CW spectrum provides static properties, like the interfacial stiffness or the interfacial free energy [12, 13].

At smaller length scales and higher frequencies, the surface of elastic media exhibit thermal excitations known under the name of Rayleigh waves [14]. These are small amplitude, high frequency perturbations that result from the elastic response of the solid.

Rayleigh and CW serve as a benchmark for the study of other surface phenomena in more complex materials. For example, polymer solutions and polymer gels, which are able to support both elastic and viscous response, exhibit a crossover from capillary to elastic SW [15–17]. The CMI also appears as an interesting system for the observation of SW. The solid phase is elastic and could in principle exhibit Rayleigh waves, while the fluid phase is viscous and could rather favour CW.

Unfortunately, despite the fair amount of theoretical research in the field, there seems to be no appropriate theoretical framework for the study of crystal-melt SW dynamics. Pleiner, Harden and Pincus extended the Rayleigh theory in order to incorporate the viscoelastic response of polymeric materials, but did not consider polymers in contact with a viscous dense phase [18, 19]. The theory was later extended to study a dense fluid on an elastic medium, but capillary forces were neglected [20]. On the contrary, Jeng et al extended the Kelvin theory to study SW at the interface of two dense fluids, but did not incorporate the elastic response of the solid [6]. A suitable theoretical framework is in principle that of Baus and Tejero, who considered SW at the interface of two fluids baring simultaneously viscous and elastic response. However, the final results were worked out only for the special case of a vapour-liquid interface where one of the phases has negligible viscosity [5, 21].

An alternative rather different approach to study interfacial fluctuations of the crystal-melt interface is employed in the field of crystal growth. The emphasis here is on the hydrodynamic equations of heat and mass transport, and energy dissipation is enforced by introducing gaussian random noise. In the limit of small temperature gradients, this formalism provides a diffusion equation for the interface height fluctuations, and hence a strongly damped interface dynamics [7, 8, 22].

Computer simulations (see e.g. Ref. [23] and references therein) and experiments of colloidal systems

[13] have also been used to investigate the CMI. Both approaches allow for the visualization of the CMI at a single-particle scale. Therefore, these techniques are highly suited to improve our understanding of the CMI. Many studies are devoted to obtain relevant static properties of the interface, such as the stiffness or the interfacial free energy, by means of an analysis of the spectrum of interface fluctuations (e.g. [12, 23–27]). The interfacial free energy can also be obtained by other methods like thermodynamic integration [28–32], metadynamics [33], or by combining classical nucleation theory with simulations [34–36]. The study of dynamic properties of the CMI, by contrast, has not received that much attention. The dynamics of the CMI has only been investigated by means of computer simulations for metal models [8] and hard spheres [22], and experimentally for colloidal suspensions [13]. Not only there are just a handful of works dealing with the dynamics of the CMI but the results are in some cases contradictory. For instance, in simulation studies [22] a quadratic dependency of the relaxation frequency with the wave vector is observed whereas the experimental work of Ref. [13] claims that such dependency is instead linear.

Motivated by the importance of gaining a deeper understanding on the dynamics of the CMI we pursue in this paper a computer simulation study of the relaxation of SW for the CMI of three archetypal systems, namely hard spheres (HS), Lennard Jones (LJ) and water. We show that the relaxation of crystal-melt SW is well described by a double exponential given that there are different processes, characterised by different time scales, involved in such relaxation. As the wavelength increases only one process, the relaxation of CW, is observed. We also show that the details of the microscopic dynamics are not important for the relaxation of crystal-melt CW. Moreover, we compare the relaxation dynamics of SW for systems composed of molecules with (water) and without (LJ and HS) orientational degrees of freedom. Finally, following the methodology proposed in Refs. [7, 8], we estimate the kinetic coefficient (the proportionality constant between the speed of crystal growth and the supercooling) from our measurements of the CW relaxation dynamics, and compare our results with independent measurements of such parameter.

II. METHODS

We simulate a solid in equilibrium with its melt and characterize the dynamics of the SW. To do that we first generate an initial configuration, then simulate the system at coexistence and finally analyze the trajectories generated in our simulations. Below we give some details about this procedure.

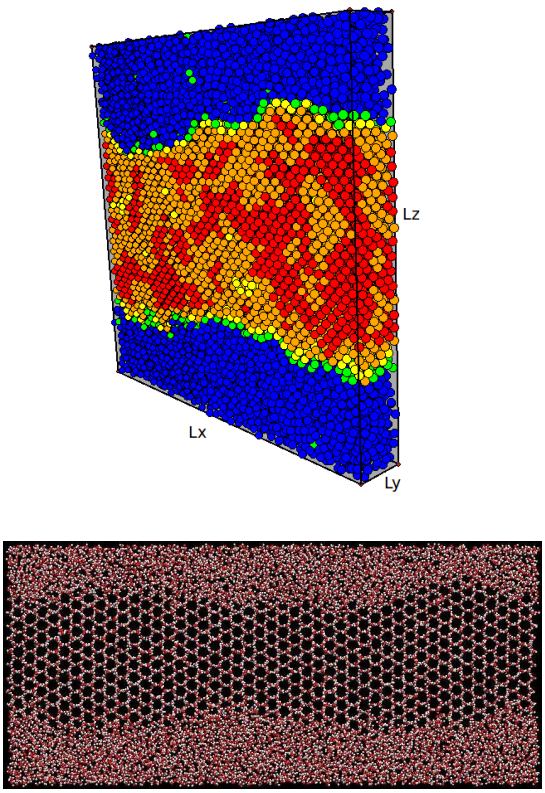

FIG. 1. Snapshots of the initial configuration for one of the LJ (top) and one of the water systems studied (bottom). In the LJ system particles are coloured according to the extent to which their local environment resembles that of an fcc lattice (in decreasing order of fcc-like character: red, orange, yellow, green and blue).

A. Generation of the initial configuration

The first step consists in creating an initial configuration. Snapshots of an initial configuration for LJ and water are given in Fig. 1. In the snapshot corresponding to the LJ system we show the way we refer to the edges of the simulation box, L_x, L_y and L_z. By preparing systems as indicated in Fig. 1 we study the dynamics of the CMI for the crystal face exposed in the x-y plane and SW propagating along the x direction. This sort of box geometry has already been used in a number of simulation studies of the CMI (see, e. g., Refs. [12, 24, 25, 37]). To specify the crystal orientation we indicate in parenthesis the Miller indexes of the interfacial plane $(x-y)$, and in square brackets the Miller indexes of the crystalline plane parallel to the direction of propagation and perpendicular to the interface $(x-z)$.

In Table I we summarize the orientation and the size of the systems investigated.

To generate the initial configuration we first start by equilibrating the solid phase with an NpT simulation at the coexistence pressure and temperature. For the equilibration of ice, ordinary Monte Carlo moves were supplemented with full ring reorientation in order to properly

Model	Orientation	L_xxL_yxL_z (σ^3)	Molecules
HS	(100)[001]	47.046x4.705x47.046	10256
	(110)[001]	44.359x4.705x52.058	10726
LJ	(100)[001]	49.101x6.336x49.181	14748
	(111)[11$\bar{2}$]	50.524x6.7313x49.292	16160
TIP4P/2005	(basal)[prismI]	59.418x5.710x29.541	10112
	(prismI)[basal]	57.024x6.962x25.581	10240
	(prismII)[prismI]	58.150x5.710x26.569	8896
	(prismII)[basal]	56.959x6.979x26.552	10670

TABLE I. Orientation and size of the systems investigated.

Property	HS	LJ	TIP4P/2005
T	-	1.0 ϵ/k_B	252 K
p	11.54 $k_BT\sigma^{-3}$	4.95 $\epsilon\sigma^{-3}$	1 bar
ρ_c	1.0369 σ^{-3}	1.005 σ^{-3}	0.921 gcm^{-3}
ρ_l	0.9375 σ^{-3}	0.923 σ^{-3}	0.993 gcm^{-3}

TABLE II. Coexistence values for the temperature, the pressure and the density for the different models. The values for the HS, LJ, and TIP4P/2005 models were taken respectively from Refs. [41], [32] and [42].

sample the hydrogen bond network [38, 39]. The final snapshot of the bulk solid thus equilibrated is rescaled so that the density matches the average equilibrium density. It is important to set L_x and L_y equal to their respective equilibrium values to avoid the solid being stressed in the x-y plane [40]. Then, a configuration of the fluid phase is equilibrated in an Np_zT simulation in a box with the same edges L_x and L_y as the equilibrated solid. In the Np_zT ensemble the pressure is exerted along the z direction. In this way, the box keeps the sides L_x and L_y fixed so it can be subsequently glued to the equilibrated solid along the x-y plane. The fluid is equilibrated at the coexistence temperature and at a pressure higher than the coexistence pressure. After equilibration of the fluid, we bring the solid and the fluid boxes together and remove the fluid particles that are less than a diameter apart from any solid particle. This causes a small drop in the fluid's density, which is partly compensated by the fact that the fluid was equilibrated at a pressure higher than the coexistence pressure. Finally, the system is further equilibrated in the Np_zT ensemble at the coexistence temperature and pressure to ensure that the fluid's density fully relaxes to its coexistence value. The overall density of the initial configuration thus generated must lie in between the densities at coexistence of the liquid and the solid (in Table II we summarize the coexistence conditions for the three models investigated).

B. Simulation details

Once we have an initial configuration, production runs are carried out in the NVT ensemble. Given that the overall density of the system lies in between the coexistence densities of the two phases, the interface is stable in an NVT simulation at coexistence temperature.

In principle, NVE simulations provide correct trajectories that preserve local momentum conservation and yield correct hydrodynamics. However, temperature control on long NVE simulations is difficult, particularly for systems exhibiting two phase coexistence. Of course, a sufficiently small time step can always be chosen that will garantee numerical stability in a single, long NVE run, but this would result in prohibitively large CPU time. A possible strategy would be to obtain independent configurations of the crystal-melt interface in a long NVT simulation and use such configurations for short production runs in the NVE ensemble. However, we find we can obtain correct results just from the long NVT simulation (see Appendix C) by using a recently developed version of the velocity-rescaling thermostat due to Bussi, Donadio and Parrinello [43]. Such thermostat, perturbs the dynamics gently by effectively rescaling the velocities over a large period and has met wide acceptance. Theoretical and numerical studies show that this thermostat requires close to minimal perturbation of the correct time evolution for given thermostating performance [44]. In practice, Bussi et al. have shown that this algorithms provides diffusion coefficients that are insensitive to the thermostating relaxation time chosen in a range spaning several orders of magnitude. Similarly, Delgado-Buscalioni et al. note that a thermostat with a sufficiently large thermalising time provides capillary wave dynamics of the liquid–vapor interface that does not differ significantly from results performed in the NVE ensemble [45]. In order to be in the safe side, we employed relatively large relaxation times of $\tau = 1ps$ and $2ps$ for the Lennard-Jones and water systems respectively. The relatively large system sizes that are required to perform our study also help to achieve correct thermostatization with minimal perturation of the dynamics [43, 44]. Moreover, for the Lennard-Jones system we have checked that changing the relaxation time from $\tau = 1ps$ to $\tau = 100ps$ does not change our results.

For the HS model, production runs were carried out using both a conventional Monte Carlo (MC) algorithm and an event driven molecular dynamics (MD) algorithm based on that provided in Ref. [46]. In order to have enough statistics we simulate ∼1000 trajectories starting from different initial configurations for MD simulations and ∼250 for MC. Every MD trajectory is run for $\sim 4\times10^6(\sigma^2m/k_BT)^{\frac{1}{2}}$, where σ is the particle diameter, m the mass and k_B the Boltzmann constant. For MC simulations we performed $1.5{\cdot}10^6$ MC cycles where each cycle consists in an attempt of centre of mass displacement per particle. The maximum displacement for the centre of mass was set to $3.8{\cdot}10^{-2}\sigma$. In each trajectory

(both MD and MC), 150 configurations were saved in a logarithmic time scale to perform the subsequent analysis.

To simulate water we used the MD GROMACS package [47, 48] and the TIP4P/2005 water model [49]. The time step for the Velocity-Verlet integrator was fixed to 0.003 ps and snapshots were saved every 75 ps. Simulations were run for a total time of $\sim 0.5\mu s$. The temperature was set to 248.5 K. At this temperature, very close to the melting value of 252 K reported in Ref. [49], we found no significant drift of the average height of the ice-water interface.

The LJ system was simulated using the MD GROMACS package. We use the truncated and shifted LJ potential proposed by Broughton and Gilmer [50]. We simulate the GROMACS implementation for Ar: $\sigma = 3.405$ Å, $\epsilon/k_B = 119.87$K, $m = 6.69 \cdot 10^{-26} kg$. The time step for the Velocity-Verlet integrator was fixed to 0.01 ps and snapshots were saved every 2 ps for a total simulation time of 0.1 μs.

For the case of HS we performed several independent short trajectories, whereas for water and LJ we opted for running just one long simulation for each investigated interface.

In order to be able to compare the relaxation dynamics of the different simulated systems in the same time scale we define the following dimensionless time: $t^* = t6D/\sigma^2$, where D is the diffusion coefficient of the fluid at coexistence. The ratio $\sigma^2/(6D)$ is the average time it takes for a fluid particle to diffuse its own diameter and we refer to it as "diffusive time". Therefore, t^* indicates the number of times a fluid particle diffuses its own diameter. For the self diffusion coefficient of the fluid at coexistence we use $D = 0.024(k_B T\sigma^2/m)^{1/2}$ for the HS model with event driven MD [51], $D = 1.456 \cdot 10^{-5}$ σ^2/cycle for the HS model with MC simulations, $D = 3.87 \cdot 10^{-3}$ $\sigma^2 ps^{-1}$ for the LJ model (in good agreement with the value reported in Ref. [52]), and $D = 0.3865$ $nm^2 ns^{-1}$ for the TIP4P/2005 model.

C. Dynamics of the surface waves

As shown in Fig. 1, the CMI of the systems here investigated is wavy. The purpose of this work is to characterize the dynamics of such waves. To do that we first define the local interface position, or interface profile $h(x_n)$, at discrete positions x_n along the x direction (see below for further details).

The interface profile is then Fourier transformed, and Fourier modes h_q defined as:

$$h_q = \frac{1}{N}\sum_{n=1}^{N} h(x_n) e^{iqx_n} \tag{1}$$

where N is the number of discretization points along the L_x side of the simulation box, and each wave mode is associated with a reciprocal space vector, q, that can take values $q = 2\pi k/L_x$, where k is a positive natural number. Small q vectors correspond to wave modes with a large wave length and viceversa.

The time-dependent autocorrelation function of h_q is then given by:

$$f_q(t) = \frac{\langle h_q(0) h_q(t)^* \rangle}{\langle h_q(0) h_q(0)^* \rangle}. \tag{2}$$

This function gives information about the way a capillary wave mode relaxes. It depends not only on q, but also on the orientation of the crystal with respect to the fluid: $f_q(t) \equiv f(t, q, (h, k, l), [m, n, o])$. In this paper we analyze the q-dependence of $f_q(t)$ for three different models and for several orientations.

D. Determination of the interface profile, $h(x_n)$

The definition of a suitable interface profile from a set of atomic positions is a subttle matter [53, 54]. It is now well understood that the evaluation of the function $h(x_n)$ consistent with the capillary wave model requires to properly identify the phase to which atoms may be attributed, and only then, searching for an optimal surface separating each phase [53, 54]. Whereas the optimal process is involving and time consuming [54], it has been observed that dynamic properties are rather insensitive to details of the specific procedure [45]. For this reason, we have chosen a simple method, inspired on that proposed in Ref. [24], that is computationally convenient and is very robust to the arbirary parameters required in practice (c.f. section III C 1).

To obtain the discrete function $h(x_n)$ describing the profile of the interface along the x direction we consider the outermost particles of the crystal slab. We first label the molecules in the system as fluid-like or solid-like. To do that we make use of local bond order parameters that are able to distinguish between fluid and solid-like particles in an instantaneous configuration by looking at the relative position of a particle with respect to its neighbours (see Appendix A for details).

Once all molecules are labelled, we remove the fluid-like particles and among all solid-like particles (red, orange, and yellow in Fig. 1 (top)) we take those that form the largest cluster. In this way we are left with the crystal phase alone. Note from Fig. 1 that due to the geometry of the system we have two independent interfaces. We explain below how we calculate $h(x_n)$ for one of them.

We start by splitting L_y in two, so the interface is divided in two elongated stripes. Each stripe is divided in N equispaced points along L_x. These points define the set of x_n values in which $h(x_n)$ is evaluated. For a point with coordinates (x_n, y_p), with $p = 1, 2$ indicating a given stripe, the local amplitude $h(x_n, y_p)$ is evaluated by averaging the z coordinate of the n_o outermost atoms with y coordinate $\in [y_p - L_y/4 : y_p + L_y/4]$ and x coordinate $\in [x_n - \Delta_x/2 : x_n + \Delta_x/2]$ (Δ_x and n_o are adjustable parameters). In this way, a function $h(x_n, y_p)$ is obtained

for each stripe, and the final $h(x_n)$ is obtained as the average between the stripes corresponding to y_1 and y_2.

Thus, the adjustable parameters to obtain a discretized profile of the interface in the way above described are N, Δx, and n_o. The results shown in the remaining of the paper correspond to the following set of analysis parameters: $N = 50$, $\Delta x = 3\sigma$ and $n_o = 4$. In section III C 1 we show that our main results are not affected by this particular choice of analysis parameters.

E. Interfacial stiffness

To test our simulations we make use of the following expression provided by Capillary Wave Theory [55, 56]:

$$\langle |h_q|^2 \rangle = \frac{k_B T}{A\widetilde{\gamma} q^2} \tag{3}$$

that relates the average squared amplitude of the capillary wave mode q, $\langle |h_q|^2 \rangle$, to the interfacial stiffness, $\widetilde{\gamma}$, by means of the equipartition theorem (note from Eq. 2 that $\langle |h_q|^2 \rangle$ is equal to the unnormalized $f_q(0)$). In the equation above k_B is the Boltzmann constant and $A = L_x L_y$ is the area of the interface. The interfacial stiffness has been carefully obtained for a number of systems [24–27], with the HS model among them. Therefore, we can double-check our results by comparing our value for $\widetilde{\gamma}$ with that obtained in Refs. [24, 27].

F. Kinetic coefficient

An important parameter in crystal growth is the kinetic coefficient, μ. The kinetic coefficient of a CMI is the proportionality constant between the speed at which the interface front advances, v, and the supercooling, ΔT:

$$v = \mu \Delta T \tag{4}$$

where $\Delta T = T_m - T$ is the the difference between the melting temperature, T_m, and the temperature of interest, T.

As shown in Refs. [7, 8], by analysing the crystal-melt CW, it is possible to obtain an estimate of μ. The method entails first obtaining $f_q(t)$ via Eq. 2 for a number of q-modes, then fitting each $f_q(t)$ to an exponential function of the type $\exp(-t/\tau_q)$ to get a characteristic decay time τ_q for each mode, and finally obtaining μ from the slope of a representation of $1/\tau_q$ vs q^2:

$$1/\tau_q = \frac{\mu \widetilde{\gamma} T_m}{\Delta h_m \rho} q^2, \tag{5}$$

where Δh_m is the molar melting enthalpy, ρ is the crystal density, and $\widetilde{\gamma}$ is the stiffness, that can be obtained via Eq. 3 by extrapolating $\widetilde{\gamma}(q)$ to $q = 0$.

Following this method, in this work we compute the kinetic coefficient for all the interfaces investigated. We compare our results for HS with those obtained in Ref. [22] using the same technique, and our results for water with those obtained in a recent publication using a different approach [57].

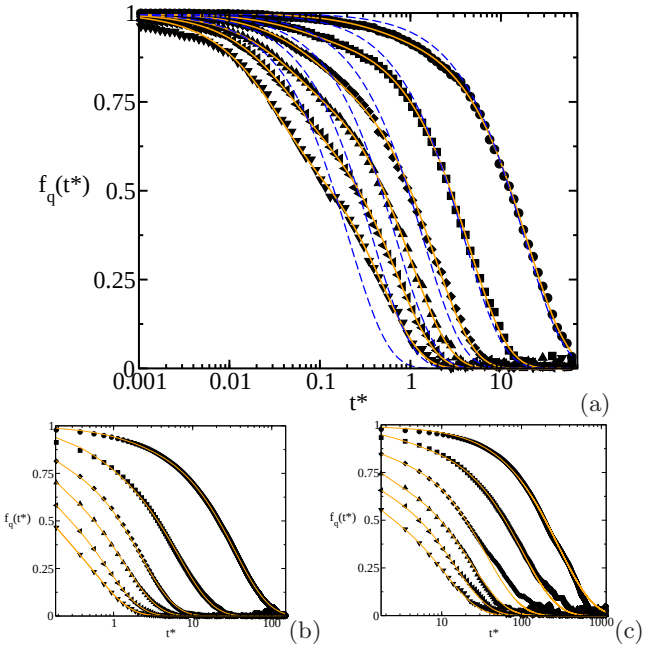

FIG. 2. (a)-(c), symbols: autocorrelation functions for the HS (100)[001], the LJ (100)[001], and the water (pII)[basal] interfaces respectively (all data correspond to MD simulations). In a given plot, curves from right to left correspond to wavevectors $q = 2\pi k/L_x$, with $k \leq 6$. Lines correspond to different fits: dashed blue to a single exponential, and solid orange to a double exponential.

III. RESULTS AND DISCUSSION

A. Dynamics of crystal–melt surface waves

For each system described in Table I we evaluate $f_q(t)$ (Eq. 2) for several values of q. Some of these autocorrelation functions are shown in Fig. 2 (a), (b) and (c) for a HS, an LJ and a water CMI respectively. As expected, the correlation functions decay from 1 to 0 as the wave-modes relax, and the relaxation for a given interface is the slower the smaller the wave vector q (or the larger the wavelength). It is also apparent that for the wavelengths studied, the surface wave dynamics corresponds to a strongly damped regime, with no signs of oscillatory behaviour in any of our the autocorrelation functions.

This is consistent with previous simulation studies of the CMI, where the decay of the correlation functions were found to be purely exponential, or at least showed a purely monotonous decay [22, 23]. Taking this into account, we first attempt to describe the correlation functions by a single pure exponential $f_q(t) = e^{-t/\tau_{exp}}$, where the characteristic decay time τ_{exp} is the only fitting pa-

rameter. However, as seen in Fig. 2 (a) (dashed blue curves), an exponential fit does not accurately describe the decay of $f_q(t)$, particularly for curves corresponding to large qs.

Considering that SW could exhibit very different behaviour at high and low frequencies, we then attempted to fit our results using a double exponential:

$$f_q(t) = Ae^{-t/\tau_{ds}} + (1-A)e^{-t/\tau_{df}}, \qquad (6)$$

where A, τ_{ds} (characteristic time for a slow relaxation process) and τ_{df} (characteristic time for a fast relaxation process) are the fitting parameters. As it can be seen in Fig. 2 (a) (orange solid lines) this fit accurately describes all curves and is significantly better than a single exponential (we also tried fitting our results to a stretched exponential, but the resulting fit was not as good as that of a double exponential and is not shown). The double exponential fit does a good job for all systems investigated. To illustrate this, in Figs. 2(b) and (c) we show the correlation functions alongside their corresponding double exponential fits for the LJ (100)[001] and the water (pII)[basal] interfaces respectively. For the case of water the simulations are slower than for the other systems and gathering statistics to obtain quality data for $f_q(t)$ at long times is a very involving task. As a consequence, the values of $f_q(t)$ for the ice-water interface at long times are rather noisy and have not been taken into account to obtain the fits shown in Fig. 2(c).

The adequacy of the double exponential fit suggests the existence of two distinct relaxation time scales: a fast one responsible for the initial decay and a slow one responsible for the decay at long times. The presence of two simultaneous relaxation time scales resembles the behaviour observed at the interface of viscoelastic materials [5, 15–19], where a high frequency relaxation process is related to elastic Rayleigh waves, while that of low frequency is related to CW. Indeed, it has been shown that both elastic Rayleigh waves and capillary Kelvin waves may exhibit an overdamped regime where oscillations are completely suppressed and the relaxation is exponential [5]. By analogy, we assume in principle that the two different time scales found in our study for the CMI are associated to different relaxation mechanisms.

The parameter $A \in [0:1]$ in Eq. 6 quantifies the weight of each mechanism in the relaxation of CMI waves. When A is close to 1 the decay of $f_q(t)$ is dominated by the slow process and when it approaches 0.5 the decay of $f_q(t)$ is affected by both slow and fast processes. In Fig. 3 we plot A as a function of q for all systems investigated. In all cases A is close to 1 for the smallest q investigated and decreases as q increases. Therefore, we observe a relaxation essentially dominated by the slow process at low q (large wavelengths) and affected by both slow and fast processes at large q (small wavelengths).

We first attempt to elucidate the nature of the slow relaxation process by analysing the dependence of τ_{ds} on q. By carefully fitting our autocorrelation functions $f_q(t)$ to Eq. 6 we obtain $\tau_{ds}(q)$ (Note that obtaining meaningful parameters from a double exponential fit is not trivial. We had to address this issue carefully and give some indications of the fitting procedure in Appendix B). In Fig. 4 (a) we represent τ^*_{ds} versus q for all interfaces investigated. In a double logarithmic scale it appears that all curves are parallel to each other within the accuracy of our calculations. This suggest the existence of a power law of the type $\tau_{ds} \propto q^{\alpha}$, with the α exponent common to all systems. A power law is an indication that there is a common mechanism underlying the slow relaxation process of all interfaces investigated. This is remarkable taking into account the different nature of the systems here studied. A visual inspection of the relaxation of large wavelength SW, those more clearly affected by the slow process, suggests that such process can be identified with the continuous recrystallization and melting taking place at the interface (see online movie [9]).

In 1993 Karma published a theory for the relaxation dynamics of crystal-melt CW based on a diffusion equation of the interfacial profile [7]. Karma's theory predicts a power law relation between a characteristic relaxation time and q. The obtained theoretical value for the exponent is $\alpha = -2$. In Fig. 4 (a) we include a dashed line with slope -2 in the double logarithmic representation. Within the accuracy of our calculations all curves look parallel to the dashed line. Therefore, the dynamics of the slow process is consistent with Karma's theory [7]. This implies that we can identify the slow process with the relaxation of CW. In other words, the slowly relaxing SW are in fact CW. The description of the relaxation of CW via a diffusion equation in Ref. [7] is consistent both with the view inferred from our movies that the slow process is due to the recrystallization/melting at the interface and with the absence of oscillations in our $f_q(t)$s.

The theory of Karma has been previously tested in simulations of metals [8, 23, 58, 59] and HS [22]. In these works it was suggested that the relaxation of crystal-melt SW can be approximated by a single exponential for all qs. Our results above show that the scenario is more complex due to presence of fast relaxation processes that clearly affect large q modes.

We can gain further insight into the nature of the slow process by studying the relaxation of the HS CMI with MC simulations. In Fig.4 (a) we compare the slow relaxation times, in diffusive units, of HS as obtained by MD and MC simulations. The data coming from both simulation techniques lie on top of each other. The agreement between both simulation techniques is further confirmed in Fig. 5, where we compare the whole autocorrelation function for several qs. The superimposition between MC and MD curves in diffusive time units points out the relevance of the diffusive time scale for the relaxation of CMI SW. Moreover, we can tell from the good agreement between MC and MD that the microscopic dynamics is not playing any significant role in the relaxation of CMI CW. This finding strongly contrasts with the case of the fluid-fluid interface [6, 45], although it not so surprising if one takes into account that the crystal has an infinitely large

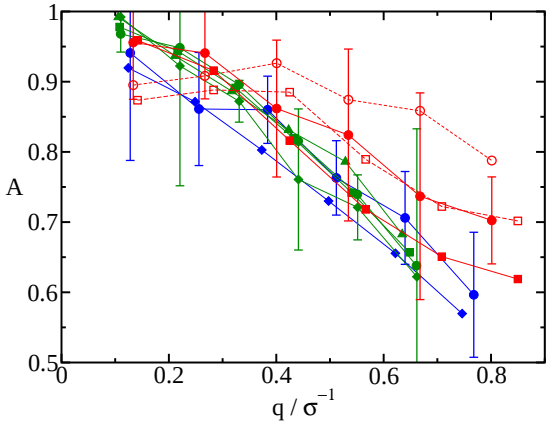

FIG. 3. Prefactor for the double exponential fit (see main text) as a function of q for all systems investigated. HS, LJ and water data are shown in red, blue and green respectively. HS data are shown for the (100)[001] (circles) and (110)[001] (squares) interfaces; LJ for the (100)[001] (circles) and (111)[11$\bar{2}$] (diamonds) interfaces; and water for the (basal)[prismatic I] (triangles), (prismatic I)[Basal] (circles), (prismatic II)[prismatic I] (squares) and (prismatic II)[basal] (diamonds) interfaces. For the HS system filled (empty) symbols and solid (dashed) lines correspond to MD (MC) simulations. Error bars are shown for one of the orientations of each model potential. Different orientations of the same model have similar error bars but have not been shown for clarity.

viscosity.

As mentioned in the introduction, we are not aware of a hydrodynamic theory of CW for the CMI. For lack of a better theoretical framework, we discuss here our observations in the context of the CW theory for either a dense or a viscoelastic medium with air [5, 6, 11]. Such systems present first a weakly damped regime at low q, with a damped oscillatory behavior of frequency $\omega \propto q^{3/2} + iq^2$ (Kelvin waves). At larger wavelengths, there is a crossover to a strong damping regime, where the oscillations are completely supressed and the frequency becomes purely imaginary $\omega \propto iq$. In our simulations, we observe only a strongly damped regime, but, at odds with standard theories for the liquid–vapor interface, the damping is not linear in q, but rather, decays as q^2. Our observation does not rule out the possibility of the aforementioned regimes occurring at smaller wavevectors than are accesible to our simulations. However, it is clear that the damping regime we observe is not the standard overdamped regime linear in q that has been reported elsewhere for the liquid-vapor interface [45]. Also note that a recent experimental study of the CMI of strongly repulsive colloids reported relaxation dynamics in agreement with a linear q dependence [13], but neither our results nor those of Ref.[22] seem to support this conclusion. Interestingly, Jeng et al. noticed in their hydrodynamic theory of surface waves a strongly damped regime with purely imaginary frequency which has both a quadratic and linear contribution in q. However, we do not observe any signature of mixed quadratic and linear dependence in our relaxation times either. Possibly, only a hydrodynamic theory incorporating both the viscous behavior of the liquid and a viscoelastic response of the crystal can predict the behavior observed in our simulations [5].

Fig. 4 (b) displays the characteristic times for the fast relaxation process, τ^*_{df}, as a function of the wave vector. For a given q, τ^*_{df} is one or two orders of magnitude lower than τ^*_{ds}. Both τ^*_{df} and τ^*_{ds} decrease as q increases. Altghouh the error bars for τ^*_{df} are quite large, it seems that a power law is not evident from Fig. 4 (b). This suggests that the fast relaxation can not be identified with a single process but rather with a combination of different ones. Such processes must be fast as compared to the diffusion of the interfacial front ($\tau^*_{df} << \tau^*_{ds}$) and must cause small perturbations in the interfacial profile (their effect vanishes as q goes to 0, as shown in Fig. 3). Having these characteristics in mind, processes such as Rayleigh SW, subdiffusion of the fluid, or the attachment/detachment of single particles to/from the crystal phase are likely to lie behind the fast relaxation of the interface.

In summary, the relaxation of SW is best described by a double exponential in the q-range analyzed in this paper. This is indicative of the existence of two distinct relaxation time scales. The slow one corresponds to the overdamped relaxation of CW by diffusion of the interfacial front (the counterpart of overdamped CW for the fluid-fluid interface, although with a different $\tau(q)$ dependence). The fast one is due to quick, small perturbations of the interface profile possibly caused by Rayleigh waves, subdiffusion, and the attachment/detachment of particles to/from the crystal. In the limit of $q = 0$ the decay of $f_q(t)$ can be entirely described by a single exponential function corresponding to the slow relaxation process.

We conclude this section by comparing the slow relaxation of different systems. Such comparison is enabled by the use of a common time unit: the diffusive time. It is evident from figure 4 (a) that the curves corresponding to water lie about an order of magnitude above those corresponding to LJ or HS. This implies that, for a given q, the water interface requires roughly ten times as much diffusive time units as LJ or HS particles in order for the interface to relax. For instance, for the smallest studied q ice-water CW take to relax the time needed for a molecule to diffuse about 300 times its own diameter, while it only takes about 30 times for the LJ or the HS systems. This difference in time scales is most likely related to the fact that water molecules, contrary to the case of LJ or HS particles, have orientational degrees of freedom and need to be properly oriented to accommodate into the crystal phase.

B. Kinetic coefficient

As explained in Sec. II F, the kinetic coefficient, μ, can be estimated by measuring the autocorrelation function $f_q(t)$ for a few CW modes [7, 8]. Using this methodology Amini et al. estimated μ for the HS system [22]. In Fig.

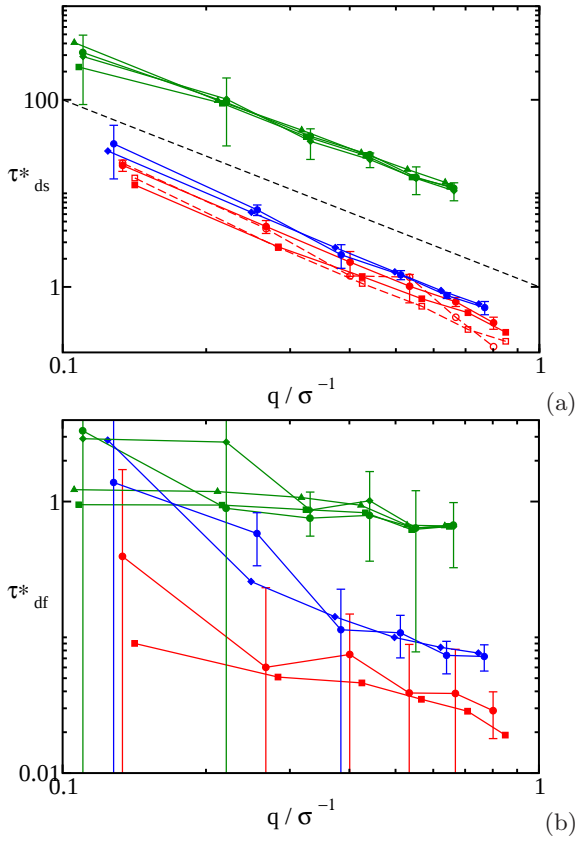

FIG. 4. (a) Dimensionless characteristic time for the slow relaxation process, τ^*_{ds}, plotted against the wave vector q in a double logarithmic scale for all interfaces investigated. Color code same as in Fig. 3. (b) Same as (a) but for the fast relaxation process. The dashed line, included in (a) for visual reference, corresponds to a power law of the type $\tau_{ds} \propto q^{-2}$.

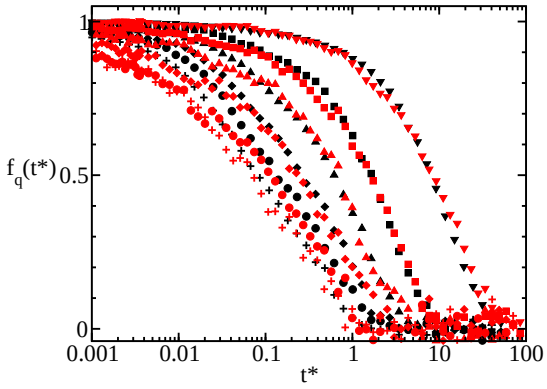

FIG. 5. Autocorrelation functions for the (110)[001] HS interface obtained by MD (black) and MC (red) simulations. From right to left functions corresponding to wavevectors $q = 2\pi k/L_x$, with $k \leq 6$, are represented.

6 (a) and (b) we plot the inverse of the relaxation time versus q for an interface of the HS system and compare our results (filled circles) with those of Ref. [22] (filled squares). From the slope of the plot shown in Fig. 6 one can obtain μ via Eq. 5. (Alternatively, as shown in Fig. 6 (c), a representation of $\tau_{ds}q^2$ vs q gives a horizontal line from which μ can be obtained). As shown in Fig. 6, the agreement with Ref. [22] is quite satisfactory, which gives us great confidence in our calculations. The filled circles in Fig. 6 were obtained by fitting our $f_q(t)$s to Eq. 6 in order to get the characteristic time τ_{ds}. If we get the characteristic relaxation time by fitting $f_q(t)$ to a simple exponential function, disregarding the fact that there are two distinct time scales involved in the relaxation of crystal-melt SW, we get the empty circles in Fig. 6, that are not in good agreement with Ref. [22]. Although, to the best of our knowledge, the need of fitting $f_q(t)$ to a double rather than to a single exponential is pointed out for the first time in this work, previous studies that assumed a single exponential behaviour provide results that are consistent with ours [22]. This apparent contradiction is explained by the fact that in Ref. [22] the characteristic time was obtained from the slope of the linear regime in a plot of $\ln f_q(t)$ vs. t [22], which, for long times, gives the characteristic time for the slow relaxation process (note that eq. 6 can be approximated by a single exponential for long times given that $\tau_{ds} >> \tau_{df}$). Such decoupling between the fast and the slow process is less and less evident as the relaxation of the q modes becomes faster or, equivalently, as q increases. Therefore, in order to consider large qs for the calculation of μ from a plot like that shown in Fig. 6 it is advisable to use Eq. 6 to obtain the characteristic time for the slow relaxation process. In fact, with our analysis we are able to extend the linear regime of $1/\tau_{ds}$ vs q^2 to larger qs than in Ref. [22].

In Fig. 6 (b) we show a $1/\tau_{ds}$ vs. q^2 representation for the LJ (left) and water (right) systems. All interfaces show, within the accuracy of our measurements, a linear dependency of $1/\tau_{ds}$ vs. q^2. This result had already been anticipated in Fig. 4 (all data sets are parallel to the dashed line). From the slopes in Fig. 6 we estimate the kinetic coefficients, which we report in Table III. Since we reduce time by the diffusive time (see Sec. II B) and distance by the particle diameter, the kinetic coefficient in our reduced units tells us how faster the interface advances, in terms of diameters per diffusive time, when the temperature is lowered by 1 K. The data in Table III reveal that the kinetic coefficient of water is more than an order of magnitude lower than that of LJ. This means that one would need to supercool water ten times more than LJ to get the same speed-up of the interface advance measured in diameters per diffusive time. Our work shows that both the relaxation and the growth of the interface are dramatically slowed down for the case of water, probably due to the role of orientational degrees of freedom in crystallization.

We can also compare our results for water with experimental [60] and simulation [57, 61] measurements of the speed of crystal growth, v. Using Eq. 5 and knowing that $v = 0$ for $\Delta T = 0$ we can estimate v *in the vicinity* of the melting temperature from our calculated μ. In Fig. 7 we plot v versus the supercooling, ΔT, for the basal

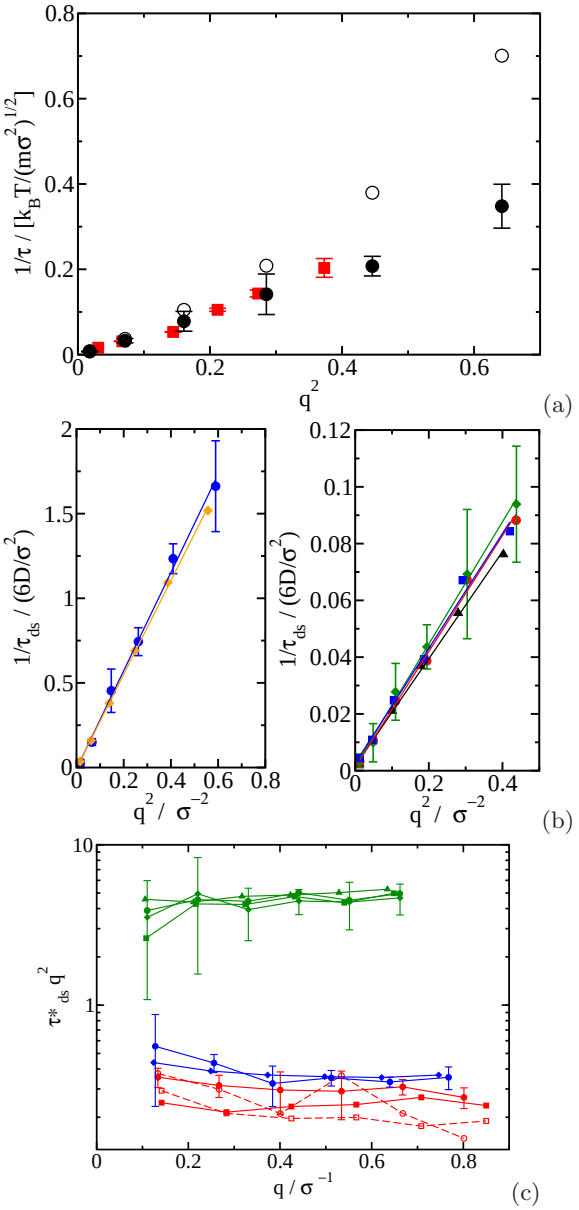

FIG. 6. Plots of the inverse relaxation time versus q^2. From the slope of these plots the kinetic coefficient can be inferred via Eq. 5 [7, 8]. In (a) our results for the (100)[001] HS interface (circles) are compared to those reported in Ref. [22] (squares). Empty (solid) circles correspond to relaxation times estimated by fitting $f_q(t)$ to a single (double) exponential. In (b) we show our results for all interfaces investigated for the LJ (left) and the water (right) systems respectively. (c): $\tau^*_{ds} q^2$ as a function of q in a logarithmic scale for all interfaces investigated. Color code same as in Fig. 3

plane of water, for which we obtained a kinetic coefficient $\mu = 1.6\ cm/(sK)$. Our results correspond to the dashed line in Fig. 6. A negative v means that the interface recedes because the crystal melts for $\Delta T < 0$. The red solid curve corresponds to the simulation results reported in Ref. [57] (large system), where $v(T)$ for the basal plane was measured by monitoring the height of the interface along time for different temperatures. Remarkably, our

Model	Orientation	$\mu/[6D/(\sigma K)]$
LJ	100	$(8 \pm 2)\cdot 10^{-2}$
	111	$(5.8 \pm 0.6)\cdot 10^{-2}$
TIP4P/2005	basal	$(2.1 \pm 0.3)\cdot 10^{-3}$
	prismatic I	$(3.0 \pm 0.4)\cdot 10^{-3}$
	prismatic II	$(2.5 \pm 0.5)\cdot 10^{-3}$

TABLE III. Kinetic coefficient, μ, for the LJ and TIP4P/2005 systems.

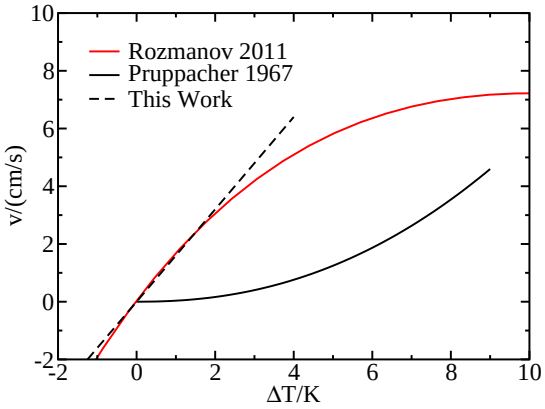

FIG. 7. Rate of crystal growth versus supercooling. We compare our results (dashed line) with the simulation results of Rozmanov et al. [57] (red solid curve) and with experimental data by Pruppacher [60] (black solid curve).

estimate of v around the melting temperature is in very good agreement with the results of Ref. [57], obtained by a completely different approach. It should be noted that the proportionality law of Eq. 5 only works for a narrow temperature range around melting. Outside that range, the dependence of v with ΔT is not linear any more and even shows a maximum at $\Delta T \approx 12\ K$ [57]. Our kinetic coefficients for the prismatic I, and prismatic II planes are $\mu = 2.2\ cm/(sK)$ and $\mu = 1.8\ cm/(sK)$ respectively. The latter is consistent with a recent simulation study of the speed of crystal growth for the prismatic II plane [61]. The comparison of the model with the experiment [60], solid black curve in Fig. 7, is not as satisfactory, though. The experimental v near coexistence is much lower than that predicted by the model. Further work is needed to understand why a model that gives a good agreement with the experiment for the rate of crystal nucleation [36] is not able to accurately predict the rate of crystal growth.

C. Robustness of our calculations

In order to check if our calculations are robust we asses the dependence of our results on both the choice of the analysis parameters and the system size. Moreover, whenever possible, we compare our results with the

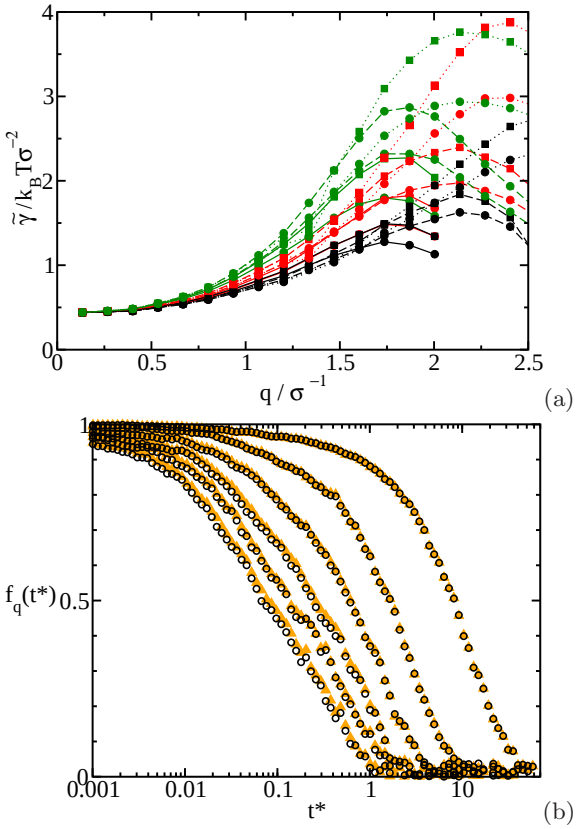

FIG. 8. (a) Stiffness as a function of q using different parameters to locate the interface for the (100)[001] HS system. $\Delta x/\sigma = 2.0$ (black), 2.5 (red) and 3.0 (green); $n_o = 3$ (circles) and 4 (squares); $N = 30$ (continuous line), 40 (dashed line) and 50 (dotted line). (b) Autocorrelation function (Eq. 2) for the (110)[001] HS system using two different sets of parameters to locate the interface: $\Delta x = 3\sigma$, $n_0 = 4$ and $N = 50$ (black circles) and $\Delta x = 2\sigma$, $n_0 = 3$ and $N = 30$ (orange triangles). From right to left wavevectors $q = 2\pi k/L_x$, with $k \leq 6$.

existing literature.

1. *Analysis parameters*

The adjustable parameters to obtain a discretized profile of the interface in the way above described are N, Δx, and n_o. To assess the extent to which the choice of these parameters affects our results we calculate the interfacial stiffness via Eq. 3 for the HS system using different sets of parameters. As shown in Fig. 8 (a) the stiffness is independent on the parameter set for small qs, as we approach the thermodynamic limit. By contrast, for large qs (short wave lengths) $\widetilde{\gamma}$ becomes dependent on the analysis parameters. This dependence is a consequence of the fact that the length scale of the waves becomes comparable to that of the discretization grid for large qs. There are sophisticated ways of dealing with this issue [62], but for our purpose it is enough to stick to the q range where $\widetilde{\gamma}$ is independent of the analysis parameters (i. e., the six smallest wave vectors).

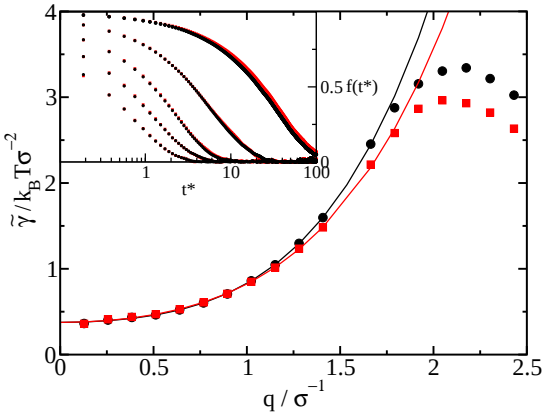

FIG. 9. Main figure: stiffness of the (100)[001] LJ interface as a function of q for two different order parameters to distinguish between solid and liquid-like particles. Black circles correspond to the order parameter described in Appendix A and red squares correspond to that described in Ref.[63]. Inset: Autocorrelation functions obtained with both order parameters for different wave vectors.

We also analyse the influence of the analysis parameters on the evaluation of the autocorrelation functions. In Fig. 8 (b) we compare $f_q(t)$ for the set of analysis parameters used in the main text ($\Delta x = 3\sigma$, $n_0 = 4$ and $N = 50$, black circles) and a completely different one ($\Delta x = 2\sigma$, $n_0 = 3$ and $N = 30$, orange triangles). Both sets of parameters give virtually identical $f_q(t)$s for the range of qs for which the dynamics has been investigated in this work ($q = 2\pi k/L_x$ for $k \leq 6$).

We have also analysed the effect that the order parameter to distinguish between crystal and fluid-like particles has in our results. In the main part of the paper we use for the LJ system the order parameter proposed in Ref. [64] with the specific parameter set given in Appendix A, whereas for the HS system we use the order parameter proposed in Ref. [65] with the parameter set given in Ref. [63]. Both order parameters are inspired by Ref. [66] and are devised to distinguish an fcc lattice from the fluid, but the order parameter of Ref. [64] gives more importance to second nearest neighbors than that of Ref. [65]. Here, we recalculate the stiffness and the autocorrelation function of the LJ system with the order parameter and set of parameters used for the HS sytem. The comparison of the results obtained with both order parameters is shown in Fig. 9. Reassuringly, the results are not sensitive to the specific choice of the order parameter, provided, obviously, that the chosen order parameter is able to distinguish between the solid lattice (fcc in this case) and the fluid.

2. *System size effects*

In order to avoid simulating systems with a prohibitively large number of molecules and yet be able to probe small-q CW we use simulation boxes with one side

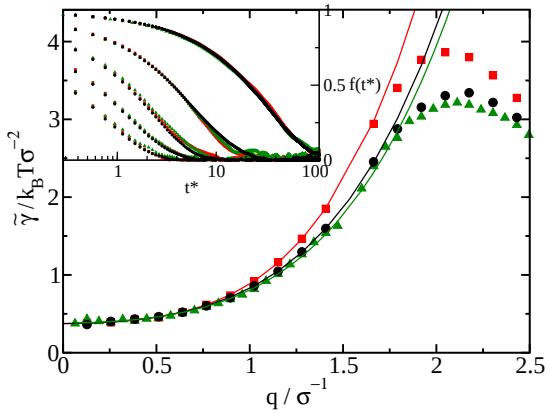

FIG. 10. Main figure: effect of the interface area in the stiffness. Black circles represent the stiffness for the (100)[001] LJ system with L_x=49.101σ and L_y=6.336σ. Green triangles and red squares represent the stiffness for the same system but with L_x'=2L_x and L_y'=3L_y respectively. Inset: Autocorrelation function for the three systems and different wavevectors.

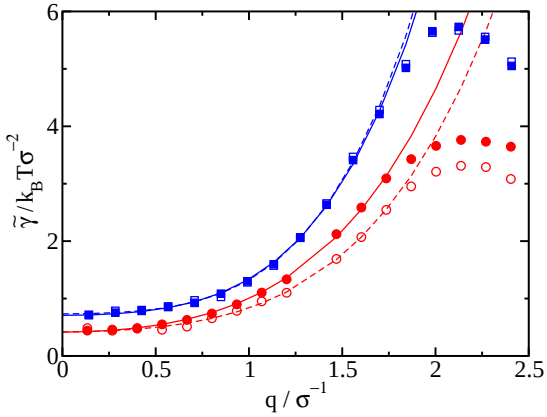

FIG. 11. Stiffness as a function of q for the HS system and two different orientations: (100)[001] (circles) and (110)[001] (squares). MC and MD results are shown with open and filled symbols respectively. The extrapolation of $\widetilde{\gamma}(q)$ to $q=0$ in order obtain $\widetilde{\gamma}$ was made by fitting $\widetilde{\gamma}(q)$ to $\widetilde{\gamma}+aq^2+bq^4$ for small qs, where a and b are fitting parameters. The fits to MC and MD results are shown as dashed and solid lines respectively.

significantly shorter than the others (see Fig. 1). This choice results in an elongated interfacial area. As shown in Ref.[25] it is advisable to check if the geometry of the simulation box introduces spurious effects in the surface wave dynamics. This is indeed a potential source of concern, since the very elongated systems employed are quasi 1–dimensional, and the behaviour of CW strongly depends on dimensionality.

In this section we provide some evidence that our choice for the shape of the simulation box does not affect our results.

To check if the typical system size we use in this work yields system-size-dependent results we take the (100)[001] LJ system and compare the results for the size reported in Table I (black circles in Fig. 10) with those obtained by making the short edge of the interfacial area (y axis) three times longer (red squares in Fig. 10). We compare both the stiffness (main Fig. 10) and the dynamic autocorrelation function (inset Fig. 10) for different wavevectors. Clearly, the typical size for the short axis of the simulation box used in this work causes no significant finite size effects for the q-range we have considered for the analysis of the dynamics ($q=2\pi k/L_x$ for $k\leq 6$). In Fig. 10 we also compare with the results obtained by doubling the long edge (x-axis) of the interfacial area (green curve). Again, no significant finite size effects are seen.

It is important to note, however, that in order to avoid system size artifacts, one must study the dynamics of the laterally averaged interface positions $h(x_n)$. On the contrary, studying the dynamics of the stripes $h(x_n, y_p)$ provides results that are strongly system size dependent.

Orientation	MC	MD	Ref.[24]	Ref.[27]
(100)[001]	0.42(2)	0.415(5)	0.44(3)	0.419(5)
(110)[001]	0.73(2)	0.707(4)	0.70(3)	0.769(5)

TABLE IV. Comparison of $\widetilde{\gamma}$ (in k_BT/σ^2) obtained in this work by means of two different simulation methodologies (MC and MD) with that obtained in previous works for the HS system and two different orientations.

3. *Consistency with previous results*

In the discussion above we have already shown that our results are consistent with previous studies. For instance, in Fig. 6(a) we show that we obtain the same kinetic coefficient as in Ref. [22] for HS. Moreover, in Fig. 7 we show that our estimate for the rate of crystal growth of ice is in good agreement with Ref. [57], where this quantity is calculated through a completely different approach. To further validate our methodology we show our results for the interfacial stiffness $\widetilde{\gamma}$ by means of Eq. 3 for two different orientations of the HS system (See Fig. 11) and compare it with previously reported values [24, 27]. The comparison is shown in Table IV. Our results are in good agreement with the literature. Moreover we obtain, as expected for an equilibrium property as $\widetilde{\gamma}$, a good agreement between MC and MD. Therefore, the way in which we simulate and analyze the interface gives results for $\widetilde{\gamma}$ that are consistent with previously published values.

IV. SUMMARY AND CONCLUSIONS

In this paper we present a computer simulation study of the crystal-melt interface for three different systems:

hard spheres, Lennard Jones and the TIP4P/2005 model of water. We focus on the dynamics of surface waves. First, we generate an initial configuration in which a crystal slab is surrounded by its melt. The box geometry allows for the study of long wave-length capillary waves without having a prohibitively large number of molecules in the system (see Fig. 1 for an example). Then, we do molecular dynamics simulations in the NVT ensemble at the melting temperature. The overall density of the system is comprised in between the coexistence densities of the fluid and the crystal phases, which guarantees that the system stays at coexistence throughout the NVT simulation. The area of the box side parallel to the interface is chosen in such way that the solid phase is free of any stress.

Once we run the molecular dynamics simulations, we analyse the dynamic autocorrelation function of the surface waves modes (Eq. 2). To do that we first obtain a function that describes the profile of the interface, which we do by identifying the outermost crystalline particles of the solid slab.

We carefully checked that our conclusions are not affected by the choice of the parameters needed to locate the interface (Fig. 8) or by the geometry of the box or the system size (Fig. 10).

We examine in detail the shape of the dynamic autocorrelation function as a function of the wave vector q, and conclude that a double exponential function describes the relaxation dynamics of crystal-melt surface waves much more accurately than a single exponential (Fig. 2 (a)). This implies that there are two distinct time scales, fast and slow, involved in the relaxation of crystal-melt surface waves. The slow time scale is due to the recrystallization-melting occurring at the interface, and is governed by capillary forces. The fast relaxation is due to a combination of processes that readily alter the shape of the interface. We speculate these may be related to Rayleigh waves, subdiffusion of the fluid and the attachment/detachment of particles to/from the crystal phase. As the length scale of the capillary wave modes increases (or q decreases) the relaxation becomes increasingly dominated by the slow process and can be just described by a single exponential. Within the uncertainty of our data, we see that the characteristic time for the slow relaxation process is related to q by the power law: $\tau \propto q^{-2}$ for all systems. Note that the conclusions obtained for the surface dynamics of the hard sphere system, which is not affected by posible artifacts from the thermsotat, fully agrees with results for the LJ and water models, where we resorted to thermostated dynamics. This power law was predicted theoretically in Ref. [7] and checked in simulations of metallic systems [8, 23, 58, 59] and hard spheres [22], although the existence of a single relaxation process was assumed in these works. Our results for hard spheres are clearly at odds with claims of a linear overdamped regime observed in the crystal–melt interface of colloids [13].

In addition to molecular dynamics simulations, we also perform Monte Carlo simulations for the hard sphere system. Monte Carlo and molecular dynamics simulations yield virtually identical autocorrelation functions if compared in diffusive time units (Fig. 5). This implies that the microscopic dynamics do not play any significant role in the relaxation of CW. Moreover, we compare the relaxation dynamics of different systems in diffusive time units. We see that the crystal-melt interface of water relaxes about ten times slower than that of hard spheres or Lennard Jones. We ascribe this difference to the presence of orientational degrees of freedom in the water molecules.

Following the methodology proposed in Refs. [7, 8] we obtain estimates of the kinetic coefficient (the proportionality constant between the rate of crystal growth and the supercooling) for all the three systems investigated. We find a good agreement with the results of Ref. [22] for hard spheres (Fig. 6 (a)). In our reduced units we can compare the kinetic coefficient for Lennard Jones with that of water. We show that a Lennard Jones crystal grows roughly ten times faster than a water crystal for the same degree of supercooling. From the kinetic coefficient we estimate the rate of crystal growth for ice at moderate supercooling. We compare it with recent calculations of such quantity obtained by a completely different approach [57, 61] and get a quite good agreement (Fig. 7). However, the linear dependence of the rate of crystal growth with the supercooling is restricted to fairly small supercooling. We also compare our results for the rate of ice growth with experimental measurements [60] and show that the employed water model predicts significantly faster rates than those seen in the experiments (Fig. 7).

Acknowledgements

We would like to thank useful discussions with R. P. Sear, R. E. Rozas, J. Horbach, A. Mijailovic, E. Romero–Enrique, R. Benjamin, and F. Monroy. E. Sanz and J. Benet acknowledge financial support from the EU grant 322326-COSAAC-FP7-PEOPLE-2012-CIG and from a Spanish grant Ramon y Cajal. L.G. MacDowell and J. Benet also acknowledge financial support from project FIS2010-22047-C05-05 (Ministerio de Economia y Competitividad).

[1] W. Boettinger, S. Coriell, A. Greer, A. Karma, W. Kurz, M. Rappaz, and R. Trivedi, *Acta Materialia* **48**, 43 (2000).

[2] D. P. Woodruff, *The solid-liquid interface*, Cambridge University Press, Cambridge, 1973.

[3] A. W. Adamson and A. P. Gast, *Physical Chemistry of Surfaces*, Wiley-Interscience, New York, 1997.

[4] H. R. Pruppacher, *J. Atmosph. Sci.* **52**, 1924 (1995).

[5] C. F. Tejero and M. Baus, *Molec. Phys.* **54**, 1307 (1985).
[6] U.-S. Jeng, L. Esibov, L. Crow, and A. Steyerl, *J. Phys.:Condens. Matter* **10**, 4955 (1998).
[7] A. Karma, *Phys. Rev. E* **48**, 3441 (1993).
[8] J. Hoyt, M. Asta, and A. Karma, *Interface Science* **10**, 181 (2002).
[9] See Supplementary Material Document No.XXX for a Molecular Dynamics trajectory for the (prismI)[basal] crystal–melt interface with the TIP4P/2005 model. Capillary waves can be seen propagating along the prismatic I plane of ice Ih and parallel to the basal plane.
[10] M. V. von Smoluchowski, *Annals of Physics* **25**, 205 (1908).
[11] L. D. Landau and E. M. Lifshitz, *Mecánica de Fluidos*, Reverté, Barcelona, 1991.
[12] J. J. Hoyt, M. Asta, and A. Karma, *Phys. Rev. Lett.* **86**, 5530 (2001).
[13] J. Hernández-Guzmán and E. R. Weeks, *Proceedings of the National Academy of Sciences* **106**, 15198 (2009).
[14] L. D. Landau and E. M. Lifshitz, *Teoria de la Elasticidad*, Reverté, Barcelona, 1969.
[15] B. H. Cao, M. W. Kim, H. Schaffer, and H. Z. Cummins, *J. Chem. Phys.* **95**, 9317 (1991).
[16] R. B. Dorshow and L. A. Turkevich, *Phys. Rev. Lett.* **70**, 2439 (1993).
[17] F. Monroy and D. Langevin, *Phys. Rev. Lett.* **81**, 3167 (1998).
[18] H. Pleiner, J. L. Harden, and P. Pincus, *Europhys. Lett.* **7**, 383 (1988).
[19] J. L. Harden, H. Pleiner, and P. A. Pincus, *J. Chem. Phys.* **94**, 5208 (1991).
[20] V. Kumaran, *J. Chem. Phys.* **102**, 3452 (1995).
[21] M. Baus and C. F. Tejero, *J. Chem. Phys.* **78**, 483 (1983).
[22] M. Amini and B. B. Laird, *Phys. Rev. Lett.* **97**, 216102 (2006).
[23] J. Hoyt, Z. Trautt, and M. Upmanyu, *Mathematics and Computers in Simulation* **80**, 1382 (2010).
[24] R. L. Davidchack, J. R. Morris, and B. B. Laird, *The Journal of Chemical Physics* **125**, 094710 (2006).
[25] R. E. Rozas and J. Horbach, *EPL (Europhysics Letters)* **93**, 26006 (2011).
[26] V. Heinonen, A. Mijailovi, C. V. Achim, T. Ala-Nissila, R. E. Rozas, J. Horbach, and H. Lwen, *The Journal of Chemical Physics* **138**, (2013).
[27] A. Härtel, M. Oettel, R. E. Rozas, S. U. Egelhaaf, J. Horbach, and H. Löwen, *Phys. Rev. Lett.* **108**, 226101 (2012).
[28] J. Q. Broughton and G. H. Gilmer, *J. Chem. Phys.* **84**, 5759 (1986).
[29] R. Handel, R. L. Davidchack, J. Anwar, and A. Brukhno, *Phys. Rev. Lett.* **100**, 036104 (2008).
[30] R. L. Davidchack, R. Handel, J. Anwar, and A. V. Brukhno, *Journal of Chemical Theory and Computation* **8**, 2383 (2012).
[31] R. L. Davidchack, *J. Chem. Phys.* **133**, 234701 (2010).
[32] R. L. Davidchack and B. B. Laird, *J. Chem. Phys.* **118**, 7651 (2003).
[33] S. Angioletti-Uberti, M. Ceriotti, P. D. Lee, and M. W. Finnis, *Phys. Rev. B* **81**, 125416 (2010).
[34] X.-M. Bai and M. Li, *J. Chem. Phys.* **124**, 124707 (2006).
[35] B. C. Knott, V. Molinero, M. F. Doherty, and B. Peters, *J. Am. Chem. Soc.* **134**, 19544 (2012).
[36] E. Sanz, C. Vega, J. R. Espinosa, R. Caballero-Bernal, J. L. F. Abascal, and C. Valeriani, *Journal of the American Chemical Society* **135**, 15008 (2013).
[37] J. R. Morris and X. Song, *J. Chem. Phys.* **119**, 3920 (2003).
[38] S. W. Rick and A. D. J. Haymet, *J. Chem. Phys.* **118**, 9291 (2003).
[39] L. G. MacDowell and C. Vega, *J. Phys. Chem. B* **114**, 6089 (2010).
[40] D. Frenkel, *arXiv:12111.440* (2012).
[41] E. G. Noya, C. Vega, and E. de Miguel, *The Journal of Chemical Physics* **128**, 154507 (2008).
[42] C. Vega and J. L. F. Abascal, *Phys. Chem. Chem. Phys.* **13**, 19663 (2011).
[43] G. Bussi, D. Donadio, and M. Parrinello, *The Journal of Chemical Physics* **126**, 014101 (2007).
[44] B. Leimkuhler, E. Noorizadeh, and O. Penrose, **143**, 921 (2011).
[45] R. Delgado-Buscalioni, E. Chacon, and P. Tarazona, *Phys. Rev. Lett.* **101**, 106102 (2008).
[46] D. C. Rapaport, *The Art of Molecular Dynamics Simulation*, University Press, Cambridge, 2004.
[47] H. Berendsen, D. van der Spoel, and R. van Drunen, *Computer Physics Communications* **91**, 43 (1995).
[48] B. Hess, C. Kutzner, D. van der Spoel, and E. Lindahl, *Journal of Chemical Theory and Computation* **4**, 435 (2008).
[49] J. L. F. Abascal and C. Vega, *The Journal of Chemical Physics* **123**, 234505 (2005).
[50] J. Broughton and G. Gilmer, *Acta Metallurgica* **31**, 845 (1983).
[51] R. L. Davidchack and B. B. Laird, *The Journal of Chemical Physics* **108** (1998).
[52] D. M. Heyes, *Phys. Rev. B* **37**, 5677 (1988).
[53] E. Chacón, E. M. Fernández, D. Duque, R. Delgado-Buscalioni, and P. Tarazona, *Phys. Rev. B* **80**, 195403 (2009).
[54] M. Jorge, P. Jedlovszky, and M. N. D. S. Cordeiro, **114**, 11169 (2010).
[55] D. Jasnow, *Rep. Prog. Phys.* **47**, 1059 (1984).
[56] D. Nelson, T. Piran, and S. Weinberg, *Statistical Mechanics of Membranes and Surfaces*, Word Scientific, Singapore, 2004.
[57] D. Rozmanov and P. G. Kusalik, *Phys. Chem. Chem. Phys.* **13**, 15501 (2011).
[58] J. Hoyt, M. Asta, and A. Karma, *Materials Science and Engineering: R: Reports* **41**, 121 (2003).
[59] J. Monk, Y. Yang, M. I. Mendelev, M. Asta, J. J. Hoyt, and D. Y. Sun, *Modelling and Simulation in Materials Science and Engineering* **18**, 015004 (2010).
[60] H. R. Pruppacher, *The Journal of Chemical Physics* **47**, 1807 (1967).
[61] R. A. Nistor, T. E. Markland, and B. J. Berne, *The Journal of Physical Chemistry B* **118**, 752 (2014).
[62] E. Chacón and P. Tarazona, *Phys. Rev. Lett.* **91**, 166103 (2003).
[63] P. N. Pusey, E. Zaccarelli, C. Valeriani, E. Sanz, W. C. K. Poon, and M. E. Cates, *Phyl. Trans. Roy. Soc. A* **367**, 4993 (2009).
[64] W. Lechner and C. Dellago, *The Journal of Chemical Physics* **129**, 114707 (2008).
[65] P. R. ten Wolde, M. J. Ruiz-Montero, and

D. Frenkel, *J. Chem. Phys.* **104**, 9932 (1996).
[66] P. J. Steinhardt, D. R. Nelson, and M. Ronchetti, *Phys. Rev. B* **28**, 784 (1983).

Appendix A: Order parameters

To distinguish between solid and liquid-like particles for the LJ and water systems we calculate for each particle a local bond order parameter, $\bar{q}_l(i)$, proposed by Lechner and Dellago [64]. If $\bar{q}_l(i)$ exceeds a certain threshold particle i is considered to be solid-like. The expression for $\bar{q}_l(i)$ reads:

$$\bar{q}_l(i) = \sqrt{\frac{4\pi}{2l+1}\sum_{m=-l}^{l}|\bar{q}_{lm}(i)|^2}, \tag{A1}$$

where

$$\bar{q}_{lm} = \frac{1}{\widetilde{N}(i)}\sum_{j=1}^{\widetilde{N}(i)} q_{lm}(j), \tag{A2}$$

and

$$q_{lm} = \frac{1}{N_n(i)}\sum_{j=1}^{N_n(i)} Y_{lm}(r_{ij}). \tag{A3}$$

Here $\widetilde{N}$ includes particle i plus all its N_n neighbours, and Y_{lm} are m^{th} order spherical harmonics. The neighbors are identified over a cut-off distance of 3.5 Å for water and 1.4 σ for LJ.

In order to determine the best choice for the order parameters we calculated the values of two order parameters, namely $\bar{q}_4$ and $\bar{q}_6$, for both the bulk solid and the bulk fluid phases at coexistence. We discuss here the case of water. As it can be seen in Fig. 12 $\bar{q}_6$ allows for a better separation between the solids (hexagonal and cubic ice) and the fluid phase in water. Next, to choose the $\bar{q}_6$ threshold ($\bar{q}_{6,t}$) that best separates the liquid from the solids, we count the percentage of mislabelled molecules in each phase for several choices of $\bar{q}_{6,t}$. Whenever a liquid particle has a $\bar{q}_6$ value larger than $\bar{q}_{6,t}$, it will be mislabelled as solid-like. Likewise, if a solid-like particle happens to have a $\bar{q}_6$ smaller than $\bar{q}_{6,t}$, it will be mislabelled as liquid-like. In Fig. 13 we plot the percentage of mislabelled molecules as a function of $\bar{q}_{6,t}$. At $\bar{q}_{6,t} = 0.3435$ the liquid and ice-Ih curves cross at a mislabeling percentage of 0.82. We choose that value as the threshold to discriminate between liquid-like and solid-like molecules. The threshold is indicated with a horizontal dashed line in Fig. 12. At $\bar{q}_{6,t} = 0.3435$ the percentage of mislabelled ice-Ic molecules is as low as 0.26. This means that ice-Ic molecules would be detected as solid-like, should they appear when the interface recrytallizes. Once molecules are labelled either as solid or as liquid-like, the largest solid cluster is found using a clustering algorithm with a cut-off of 3.5 Å to find neighbors belonging to the same cluster.

For the LJ system we used a $\bar{q}_{6,t}$ value of 0.294 and a cut-off to build the biggest cluster of 1.4σ.

For the HS system we employed an order parameter based on q_6 as described in Ref. [63] to distinguish between solid-like and liquid-like particles.

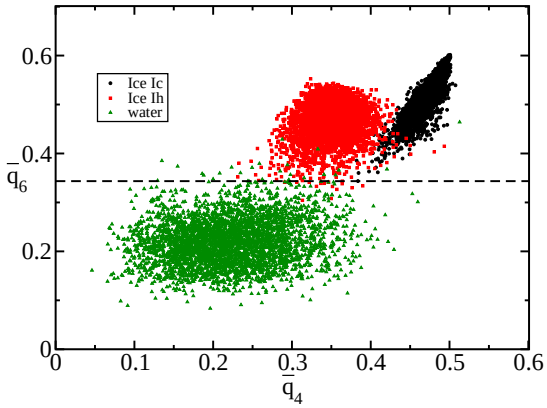

FIG. 12. Bidimensional representation of the local bond order parameters for different liquid water (green triangles), ice Ih (red squares) and ice Ic (black circles). The corresponding thermodynamic state was T=250K and p=1bar.

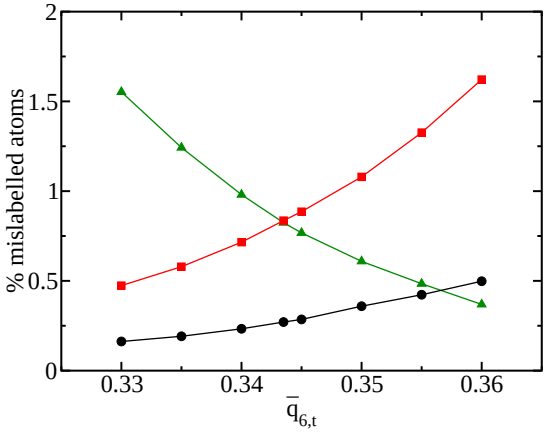

FIG. 13. Fraction of atoms mislabelled as a function of $\bar{q}_{6,t}$. Liquid water (green triangles), ice Ih (red squares) and ice Ic (black circles).

Appendix B: Double expoential fits

When fitting the time autocorrelation functions to a double exponential function (Eq. 6) it is convenient to have a good initial guess for the fitting parameters to avoid convergence to non-physical results. In order to obtain a good guess for the relaxation time of the slow process, τ_{ds}, we plot $d\ln(t)/dt$ vs t (see Fig. 14). Note that for long enough times one can approximate Eq. 6 by:

$$f_q(t) \approx Ae^{-t/\tau_{ds}}, \tag{B1}$$

taking into account that $\tau_{ds} >> \tau_{df}$. If we now take the logarithm of Eq. B1 and differenciate with respect to t we obtain:

$$\frac{d\ln(f_q(t))}{dt} \approx \frac{-1}{\tau_{ds}}. \tag{B2}$$

Therefore, from the intercept of the horizontal region of the plots shown in Fig. 14 we can get an estimate of τ_{ds}.

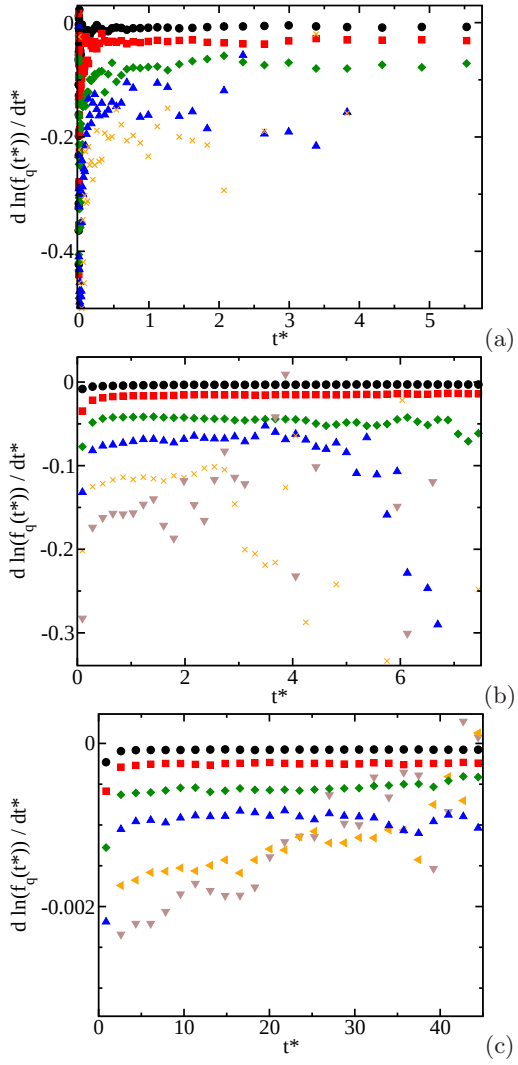

FIG. 14. Representation of $d\ln(f_q(t)/dt$ vs t for three different systems: (100)[001] HS MD (a), (100)[001] LJ (b) and (pI)[basal] TIP4P/2005 water. From top to bottom in a given plot wavevectors with values of $q = 2\pi k/L_x$ with $k \leq 6$ are shown.

Recall that the higher the q the more influenced is the relaxation of the interface by the fast process (see Fig. 3). Hence, as expected, the horizontal region in Fig. 14 becomes less evident as q increases. Nevertheless, it is enough for our purpose of getting an initial estimate for the fitting parameter τ_{ds}.

Given that for small qs the preexponential factor A is close to 1, we use $A = 1$ as an initial guess to fit the autocorrelation function corresponding to the smallest q. Regarding τ_{df}, we set an initial value two orders of magnitude smaller than τ_{ds}. We use the resulting parameters A and τ_{df} of the fit to the smallest q as an input for the following q. For τ_{ds} we use the value estimated from Fig. 14 as explained above. We repeat this process until we obtain a fit for each and every q.

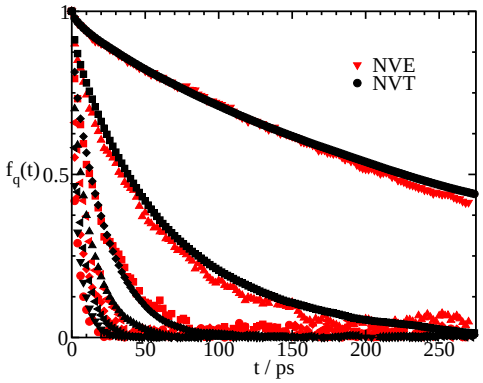

FIG. 15. Autocorrelation functions for the (100)[001] LJ system as calculated in the NVT and NVE ensembles.

Appendix C: NVE vs NVT

In Fig.15 we compare the autocorrelation functions calculated in many short NVE simulations starting from independent configurations with those obtained in a single, long NVT simulation. NVE simulations are short enough to guarantee energy conservation and, at the same time, long enough to allow for the relaxation of the studied capillary waves modes. Clearly, NVE and NVT give the same results (NVE curves are more noisy because the statistics is not as good).